Manjavacas, A.; Fenollosa Esteve, R.; Rodriguez, I.; Jiménez Molero, MC.; Miranda Alonso, MÁ.; Meseguer Rico, FJ. (2017). Magnetic light and forbidden photochemistry: the case of singlet oxygen. Journal of Materials Chemistry C. 5(45):11824-11831. doi:10.1039/c7tc04130f

Magnetic Light and Forbidden Photochemistry: The Case of Singlet Oxygen

Alejandro Manjavacas,*,† Roberto Fenollosa,‡ Isabelle Rodriguez,‡ M. Consuelo Jiménez,¶ Miguel A. Miranda,¶ and Francisco Meseguer*,‡

†*Department of Physics and Astronomy, University of New Mexico, Albuquerque, New Mexico 87131, United States*

‡*Instituto de Tecnología Química (CSIC - UPV), Universitat Politècnica de Valencia, Av. Tarongers s/n 46022, Valencia, Spain*

¶*Departamento de Química, Universitat Politècnica de Valencia, Av. Tarongers s/n 46022, Valencia, Spain*

E-mail: manjavacas@unm.edu; Fmese@fis.upv.es

Abstract

Most optical processes occurring in nature are based on the well-known selection rules for optical transitions between electronic levels of atoms, molecules, and solids. Since in most situations the magnetic component of light has a negligible contribution, the dipolar electric approximation is generally assumed. However, this traditional understanding is challenged by nanostructured materials, which interact strongly with light and produce very large enhancements of the magnetic field in its surroundings. Here we report on the magnetic response of different metallic nanostructures and its influence on the spectroscopy of molecular oxygen, a paradigmatic example of dipole-forbidden optical transitions in photochemistry.

Keywords

Plasmonics, Nanophotonics, Magnetic field, Photochemistry, Singlet Oxigen

Science and technological applications based on photochemical processes are restricted to those situations involving states of matter that are accessible through light excitation.[1] From a theoretical point of view, photochemical processes are governed by the light-matter interaction Hamiltonian, which, for material systems with subwavelength dimensions such as chemical species (i.e., atoms, molecules, etc...), can be conveniently written using a multipolar expansion of the electric and magnetic fields[2,3]

$$\mathcal{H} = -\mathbf{p}\cdot\mathbf{E} - \mathbf{m}\cdot\mathbf{B} - \mathbf{Q}:\nabla\mathbf{E} + \dots. \tag{1}$$

The first term of this expansion involves the electric dipole moment, $\mathbf{p}$, of the chemical species and, consequently, is known as electric dipole (ED) term. In a similar way, the second and the third terms contain the magnetic dipole, $\mathbf{m}$, and the electric quadrupole, $\mathbf{Q}$, moments, and therefore are known as the magnetic dipole (MD), and electric quadrupole (EQ) terms, respectively. Each of these terms presents specific selection rules that control the conditions under which the associated optical transitions can occur.[3] Usually, the electric component of an electromagnetic field is much larger than the magnetic one. For instance, for a plane wave, their ratio is $E/B = c$, where c is the speed of light. As a consequence of this, most optical processes in light-matter interaction are dominated by dipolar electric transitions.[3]

The situation is completely different when the chemical species undergoing the optical transition is placed near a metallic nanostructure. These systems are well known to support coherent oscillations of their conduction electrons, commonly known as surface plasmons, that couple strongly with light and generate large electromagnetic fields around them.[4,5] Such extraordinary properties have already been exploited in different research areas including biosensing,[6–8] photovoltaics,[9–11] and photocatalysis,[12–14] to cite some. Interestingly, the enhancement of the electromagnetic field produced by these nanostructures comes associ-

ated with a strong magnetic response[15–19] that changes dramatically the usual light-matter interaction, thus enabling new amazing phenomena such as negative refraction,[20–22] perfect lensing,[23] or even optical cloaking.[24] To this end, different structures fabricated using top-down[15,25–28] or bottom-up[29–32] techniques have been explored. These include, for instance, metallic split-ring resonators[25] and cut-wire pairs,[26,27] whose magnetic response in the optical region[33,34] has been characterized both at the single particle level[35,36] and for ordered arrays.[15,16,25–27] It is worth to note that high-refractive nanostructures can also produce strong magnetic fields, which are, in this case, associated with photonic cavity modes supported by these systems.[37–43]

The strong magnetic field produced by metallic nanostructures can be used to enhance the MD transitions of chemical species placed in their vicinity (see reference 44 for a comprehensive review). Such possibility has been theoretically explored,[45–47] and experimentally verified using principally rare-earth ions, which exhibit strong MD in the optical range associated with their $4f$ orbitals,[48–50] placed in closed proximity to plasmonic structures with different designs.[51–59] It is important to note that the strong magnetic field enhancement produced by plasmonic nanostructures in their surroundings normally comes together with an even stronger amplification of its electric counterpart,[60] which enhances the ED transitions of the chemical species. This can be very relevant for species having MD and ED transitions closely located in the spectrum, since, in these cases, the ED transition can obscure the MD transition.[61] A similar effect is expected for EQ transitions, which are enhanced by the large electric field gradients (see Eq. (1)) produced near plasmonic nanostructures.[62–66]

Among the many different chemical species that could benefit from the enhancement of the MD optical transitions provided by surface plasmons, molecular oxygen, O_2, constitutes a very relevant example. This molecule is a key specie in nature and, despite its apparent simplicity, it exhibits a number of rather unusual properties that strongly influence its spectroscopic behavior, as well as its chemical reactivity.[67] As shown in Figure 1(a), O_2 has a triplet multiplicity ground state, $^3\Sigma_g$. Conversely, its lowest lying excited states, $^1\Delta_g$ and $^1\Sigma_g$,

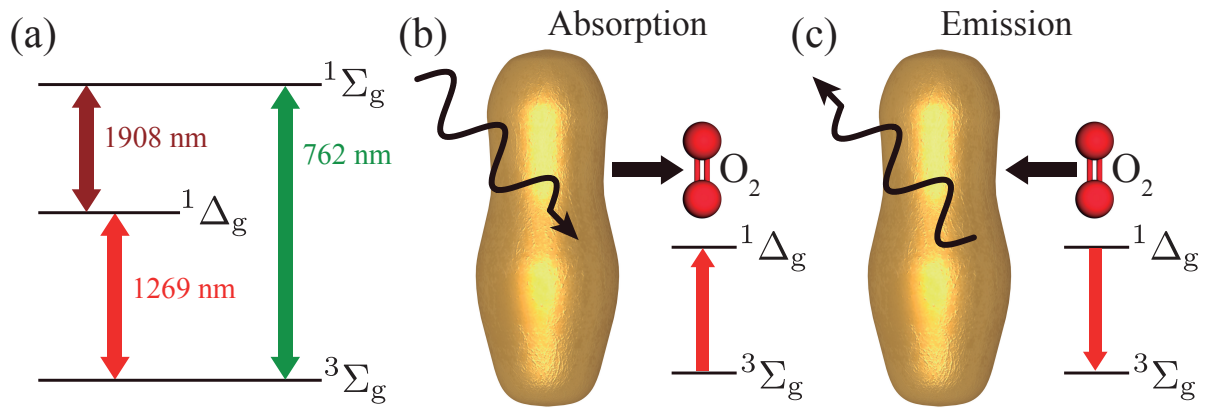

Figure 1: (a) Relevant energy levels of molecular oxygen. (b),(c) Schematics of the two optical processes that can be enhanced by the presence of a resonant metallic nanostructure: (b) an oxygen molecule absorbs a photon and is excited from the $^3\Sigma_g$ to the $^1\Delta_g$ level, (c) an excited oxygen molecule emits a photon and decays from $^1\Delta_g$ to $^3\Sigma_g$. In (b), the absorption probability is increased by the strong enhancement of the magnetic field produced by the metallic nanostructure, while in (c), the emission probability is amplified by the large scattering cross-section of the metallic nanostructure.

are of singlet nature and appear at relatively low energies above the ground state. Therefore due to spin conservation, any transition between the ground $^3\Sigma_g$ and the excited states $^1\Delta_g$ and $^1\Sigma_g$ of O_2 cannot involve the ED and the EQ terms appearing in Equation (1)[68]. Only the MD term, which is proportional to the magnetic field, can connect these levels. Such transitions are commonly referred to as forbidden optical transitions. Interestingly, their forbidden nature prevents the spontaneous photo-oxidation of living systems upon exposure to natural sunlight in an aerobic atmosphere. On the other hand, singlet O_2 is not just a relevant model for fundamental chemical and physical phenomena; it also has important applications in fields ranging from atmospheric chemistry and material science to biology and medicine, including photodynamic therapy (PDT) of cancer.[67,69] Singlet molecular oxygen exhibits a unique reactivity as synthetic reagent, as intermediate in oxygenation reactions of polymers, and as part of reactive oxygen species in a range of biological systems.[70]

Usually, the optical activation of O_2, i.e., its transition from the triplet to the singlet state, is achieved through the electronic excitation of photosensitizers, typically visible light-absorbing aromatic compounds with a high intersystem crossing quantum yield.[71] The col-

lected triplet energy is then transferred to molecular oxygen, affording the $^1\Delta_g$ and/or $^1\Sigma_g$ excited states of molecular oxygen.[72,73] Direct optical excitation is very challenging as demonstrated by the orders of magnitude of the Einstein coefficients for spontaneous emission from the singlet states, which in the gas phase are $10^{-3}\,\mathrm{s}^{-1}$, $10^{-1}\,\mathrm{s}^{-1}$, and $10^{-4}\,\mathrm{s}^{-1}$, for the $^1\Sigma_g \rightarrow {}^1\Delta_g$, $^1\Sigma_g \rightarrow {}^3\Sigma_g$, and $^1\Delta_g \rightarrow {}^3\Sigma_g$ transitions, respectively. While for O_2 dissolved in a liquid such as water, they increase to $10^3\,\mathrm{s}^{-1}$, $10^0\,\mathrm{s}^{-1}$, and $10^{-1}\,\mathrm{s}^{-1}$, respectively.[67] These numbers clearly make the excitation and deexcitation of singlet O_2 ideal optical processes that can benefit from the plasmonic enhancement of MD transitions.

In this paper, we investigate the enhancement of the magnetic dipole transitions connecting the triplet $^3\Sigma_g$ and singlet state $^1\Delta_g$ of O_2 in the presence of different metallic nanostructures. Despite the variety of optimized structures already characterized in literature, including split-ring resonators,[46] or diabolo structures,[47,74] here we choose to work with single and tip-to-tip welded gold nanorods.[75] The reason for our choice is that, in spite of their simplicity, these structures produce large magnetic field enhancements over a large volume around them, with peak values close to those of optimized nanostructures, but, as opposed to them, can be efficiently synthesized using colloidal chemistry and used in liquid suspension (customarily water), thus providing a larger region for interaction with O_2 than surface patterned nanostructures.[76] This is of vital importance to maximizing the enhancement of photochemical processes as the one investigated here. Using rigorous solutions of Maxwell's equations, we analyze the impact of these structures both in the excitation and deexcitation processes involving singlet O_2, and we discuss different potential experiments for testing the generation and detection of singlet oxygen.

Results

The two different optical processes that we consider in this work are described in Figures 1 (b) and (c). The first case corresponds to the excitation of O_2 from the $^3\Sigma_g$ to the $^1\Delta_g$

excited state by absorption of a photon. To this end, both the metallic nanostructure and the O_2 molecule are illuminated with an external light source of energy $\hbar\omega$, resonant with the transition wavelength $\lambda_0 = 1269\,\mathrm{nm}$. The probability per unit time of inducing a transition can be calculated using Fermi's golden rule[3]

$$P = \frac{2\pi}{\hbar^2} \sum_f |\langle f| \mathcal{H} |i\rangle|^2 \, \delta(\omega_i - \omega_f),$$

where $|i\rangle$ and $|f\rangle$ are the initial and final states, and and $\mathcal{H}$ is the Hamiltonian connecting them. In our case, since the transition is forbidden, the only relevant term of the Hamiltonian given in Equation (1) is the MD, and therefore the probability per unit time of absorption is proportional to $|\mathbf{m} \cdot \mathbf{B}(\mathbf{r}_0)|^2$. Consequently, the increase of this quantity due to the presence of the metallic nanoparticle is given by

$$\frac{P_\mathrm{a}}{P_\mathrm{a}^0} = \left| \frac{\mathbf{B}(\mathbf{r}_0)}{\mathbf{B}_0(\mathbf{r}_0)} \right|^2,$$

and therefore is determined by the enhancement of the magnetic field intensity at the position of the O_2 molecule produced by the plasmonic resonances supported by the metallic nanoparticle. To reproduce an experimental situation, this expression has to be averaged over all possible relative orientations between the external illumination, the metallic nanostructure, and the molecule transition dipole.

The second process considered here corresponds to the spontaneous deexcitation of O_2 from the singlet $^1\Delta_g$ state to the triplet $^3\Sigma_g$ ground state, which is sketched in Figure 1(c). In this case, the enhancement of the transition probability relative to free space can be written as[77,78]

$$\frac{P_\mathrm{e}}{P_\mathrm{e}^0} = -\frac{2\pi c^3}{\omega} \mathrm{Im}\left\{\mathrm{Tr}\, \mathcal{G}(\mathbf{r}_0, \mathbf{r}_0)\right\}, \tag{2}$$

where $\mathcal{G}(\mathbf{r}, \mathbf{r}')$ is the magnetic Green's tensor of Maxwell's equations,[79] defined as the solution

of

$$\nabla \times \nabla \times \mathcal{G}\left(\mathbf{r}, \mathbf{r}'\right) - \varepsilon\left(\mathbf{r}\right) \frac{\omega^2}{c^2} \mathcal{G}\left(\mathbf{r}, \mathbf{r}'\right) = -\frac{1}{c^2} \delta\left(\mathbf{r} - \mathbf{r}'\right),$$

with the appropriate boundary conditions. It corresponds to the magnetic field produced at $\mathbf{r}$ by a magnetic dipole placed at $\mathbf{r}'$ in the presence of the metallic nanostructure. The symbol Tr in Eq. (2) indicates the trace over $\mathcal{G}\left(\mathbf{r}, \mathbf{r}\right)$ necessary to average over all possible dipole orientations. In absence of the metallic nanostructure, P_{e} reduces to P_{e}^0, which is the Einstein coefficient for spontaneous emission of the ${}^1\Delta_g \rightarrow {}^3\Sigma_g$ transition.[79] The enhancement of the emission probability produced by the nanoparticle takes place through two different channels: radiative and nonradiative. In the first case, the nanoparticle acts as an antenna and helps to radiate the photon produced in the deexcitation of O_2. In the second situation, the nanoparticle also enhances the deexcitation process, however, in this case, the generated photon is absorbed by the nanoparticle. Since we are interested in the detection of singlet O_2 through the measurement of the emitted photons, *i.e.*, the photoluminescence, we want to enhance only the first of these two channels. Therefore, we can separate the Green's tensor into two terms: one associated with the radiative channel and the other one corresponding to the nonradiative decay: $\mathcal{G}\left(\mathbf{r}, \mathbf{r}'\right) = \mathcal{G}_{\mathrm{r}}\left(\mathbf{r}, \mathbf{r}'\right) + \mathcal{G}_{\mathrm{nr}}\left(\mathbf{r}, \mathbf{r}'\right)$. This allows us to write an expression for the photoluminescence enhancement due to the metallic nanostructure

$$\frac{P_{\mathrm{e,r}}}{P_{\mathrm{e}}^0} = -\frac{2\pi c^3}{\omega} \mathrm{Im}\left\{\mathrm{Tr}\, \mathcal{G}_{\mathrm{r}}\left(\mathbf{r}_0, \mathbf{r}_0\right)\right\}. \tag{3}$$

The photoluminiscence enhancement can be directly obtained from the calculation of the far-field emission of a classical magnetic dipole in presence and in absence of the nanostructure.

In the following, we investigate the enhancement of the absorption and the emission processes associated with the singlet O_2 molecule produced by metallic nanostructures. In particular, we focus on two different systems, namely a pair of tip-to-tip welded nanorods and a single nanorod. The geometry of the first structure resembles that of the systems traditionally considered to achieve large enhancement of the magnetic field, usually consisting

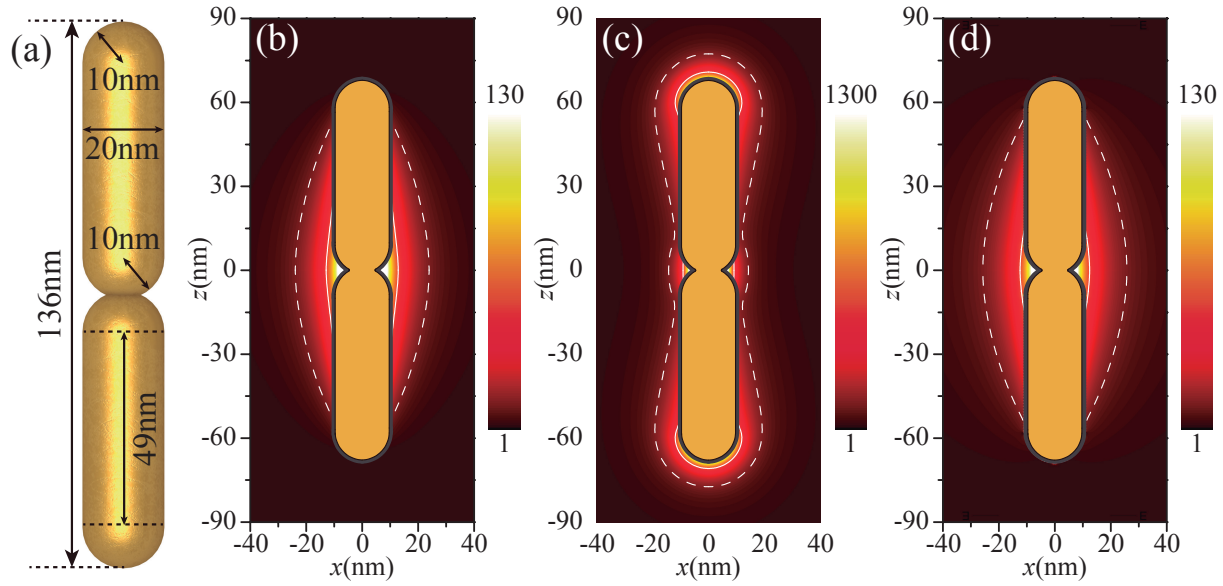

Figure 2: Optical response of a pair of tip-to-tip welded gold nanorods. (a) Geometry of the nanostructure. (b) Magnetic field intensity enhancement $|\mathbf{B}|^2 / |\mathbf{B}_0|^2$, averaged over all possible light incidence directions and polarizations. (c) Electric field intensity enhancement $|\mathbf{E}|^2 / |\mathbf{E}_0|^2$, averaged over all possible light incidence directions and polarizations. (d) Photoluminescence enhancement $P_{\mathrm{e,r}}/P_{\mathrm{e}}^0$. The dashed and solid white contours signal the regions for which the enhancement is larger than 10 and 50 for panels (b) and (d), and larger than 100 and 500 for panel (c). All calculations are performed at $\lambda_0 = 1269\,\mathrm{nm}$.

of two identical nanostructures connected by a narrow junction.[47,74] On the other hand, the single nanorod represents a simpler geometry and consequently involves a less demanding synthesis. In both cases, the dimensions of the nanostructure are chosen to ensure they support a plasmon resonant with the ${}^1\Delta_g \rightarrow {}^3\Sigma_g$ transition wavelength $\lambda_0 = 1269\,\mathrm{nm}$. Figure 2 shows the results obtained for the tip-to-tip welded nanorods. The dimensions of the nanostructure are specified in panel (a); each individual nanorod consists of a cylinder of 49 nm of length and a diameter of 20 nm terminated by two hemispheres of radius 10 nm. The two rods are welded together resulting in a structure with a total length of 136 nm. All the results discussed in the following are obtained by rigorously solving Maxwell's equations using the boundary element method (BEM).[80,81] The dielectric function for gold is taken from tabulated data,[82] and the nanostructures are assumed to be surrounded by water ($\varepsilon = 1.77$). We restrict the calculations to points separated by at least 0.5 nm from the surface of the structure. The reason is that classical calculations for points located closer to the surface are nonphysical due to nonlocal effects. Furthermore, this distance also corresponds to the typical size of molecules like cetyltrimethylammonium bromide (CTAB) that are customarily used for obtaining high aspect ratio gold nanorods and stabilizing them in aqueous suspensions.[83,84]

Upon illumination, the nanorod pair generates a strong electromagnetic field around it. Figure 2(b) shows the magnetic field intensity enhancement $|\mathbf{B}|^2 / |\mathbf{B}_0|^2$ produced by this structure, averaged over all possible incidence angles and polarizations. This enhancement can be intuitively understood by noticing that the electron oscillation associated with the longitudinal plasmon supported by the metallic nanostructure produces an electric current that, by virtue of Ampère-Maxwell's law, generates the magnetic field. The narrowing of the structure at its central region, produces an increase of the current density, and therefore an even higher enhancement of the magnetic field that can reach values above 100 near the contact point between the nanorods, and, as expected, it decays as we move away from that region. The dashed and solid white curves indicate the regions for which the enhancement

is above 10 and 50, respectively. Although here we are interested in the magnetic field enhancement, it is important to analyze the response of the electric field, and in particular its gradient since, for instance, the transition $^1\Delta_g \rightarrow {}^1\Sigma_g$, which has resonant wavelength $\lambda_0 = 1908\,\text{nm}$, is EQ allowed. Not surprisingly, the electric field is strongly enhanced near the nanostructure. In particular, as shown in Figure 2 (c), $|\mathbf{E}|^2 / |\mathbf{E}_0|^2$ can reach values above 1000, both at the contact region and at the ends of the nanorods. The dashed and solid white curves indicate, in this case, the region for which the enhancement is above 100 and 500, respectively.

The increase in the photoluminescence produced by this nanostructure is studied in Figure 2(d), where we plot the results obtained with Equation (3) for the tip-to-tip welded nanorods of panel (a). Examining these results, we observe that both the enhancement values and the spatial distribution are similar to those of the magnetic field intensity shown in panel (b). In particular, there is a significant volume around the particle for which the enhancement of the emission probability enhancement is above 10 (dashed white curve), while closer to the contact region, these values increase above 50 (solid white curves). These results are coherent with the smaller quenching near metallic structures expected for magnetic transitions as compared with their electric counterparts.[85]

Figure 3 is devoted to the analysis of the different enhancements associated to the second geometry under consideration, namely a single nanorod, whose synthesis is more direct. As shown in panel (a), the total length of the this nanostructure including the hemispheres at the ends is 156 nm, while the diameter is again 20 nm. Such dimensions are chosen to ensure the existence of a plasmon resonance at 1269 nm. Examining panel (b) we observe that the single nanorod produces similar peak values for the magnetic field intensity enhancement as the tip-to-tip welded nanorods, however this enhancement is extended over a larger volume as inferred from the comparison of the regions enclosed by the dashed and solid white curves of Figures 2(b) and 3(b). A similar behavior is obtained for the electric field (c.f. Figure 3(c)), whose extrema, in this case, appear only at the ends of the nanostructure. Regarding the

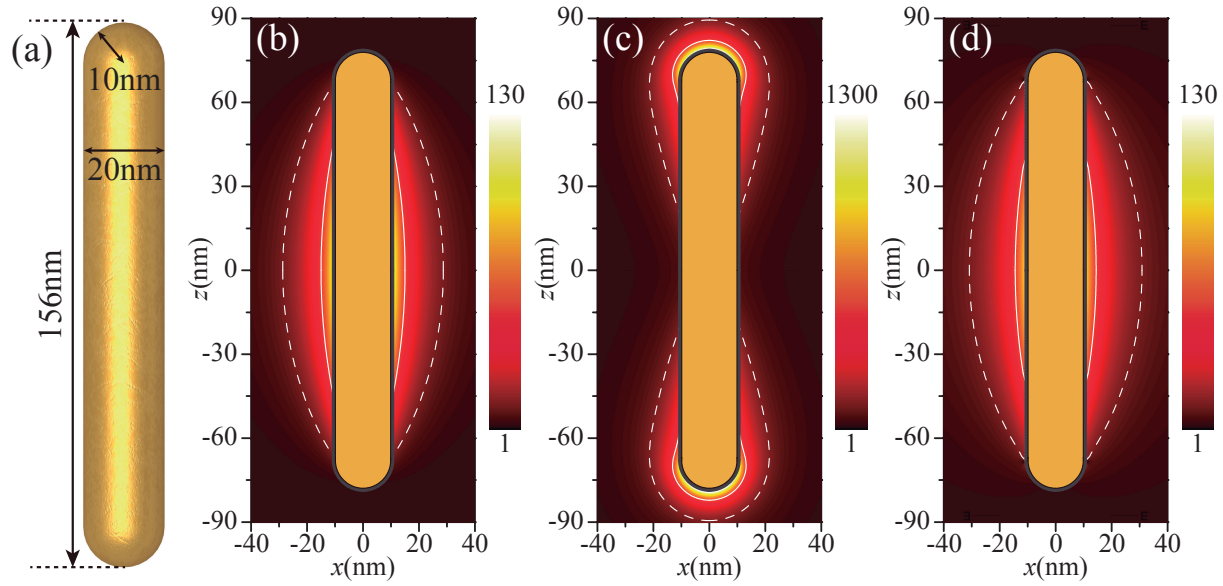

Figure 3: Optical response of a single gold nanorod. (a) Geometry of the nanostructure. (b) Magnetic field intensity enhancement $|\mathbf{B}|^2 / |\mathbf{B}_0|^2$, averaged over all possible light incidence directions and polarizations. (c) Electric field intensity enhancement $|\mathbf{E}|^2 / |\mathbf{E}_0|^2$, averaged over all possible light incidence directions and polarizations. (d) Photoluminescence enhancement $P_{\mathrm{e,r}}/P_{\mathrm{e}}^0$. The dashed and solid white contours signal the regions for which the enhancement is larger than 10 and 50 for panels (b) and (d), and larger than 100 and 500 for panel (c). All calculations are performed at $\lambda_0 = 1269\,\mathrm{nm}$.

enhancement of the photoluminescence, as shown in panel (d), it reaches values very similar to those displayed by the tip-to-tip welded nanorods of Figure 2, but extended over a larger region around the nanostructure. It is important to remark that the enhancement values provided by the structures studied here are not far from those reported for optimized planar geometries such as diabolo nanostructures once one takes into account the averaging over all possible relative orientations between the dipole and the nanostructure,[47] but with the advantage that both the single and tip-to-tip welded nanorods can be efficiently synthesized using colloidal chemistry techniques and used in liquid suspension, thus enabling much larger interaction volumes with O_2.

In the following part we discuss the potential photochemical reactions that we can carry out for sensing the generation of singlet oxygen in the presence of gold nanorods.

Discussion of the potential photochemical reactions

The formation of singlet O_2 can be monitored by steady state and time resolved absorption and/or emission measurements, as well as by chemical trapping using selected probes we describe hereafter, or even trough quartz enhanced photoacoustic spectroscopy[86]. As the photoactivation yields of different species are very low we can either use high intensity light sources, but at the risk of damaging the sample, or time accumulative experiments. We prefer the second option where the existence of a certain product in a given solution proves the photoactivation of oxygen because the chemical reaction generating such a product can only occur whenever oxygen is excited to its singlet state. It is important to notice that the rate of this chemical reaction is expected to be larger than the radiative decay rate of singlet O_2, even with the enhancement provided by the metallic nanostructure. Specifically, the following test reactions would be of interest to prove the concept (see the Supporting Information): (i) "ene" reactions to give allylic hydroperoxides, (ii) dioxetane formation through $[2+2]$ cycloadditions and (iii) $[4+2]$ cycloadditions to diene systems. The results

(reactivity, chemo-, regio- and steroselectivity) could be compared with those obtained using organic dyes as photosensitizers. An appropriate system to examine singlet oxygen-mediated photoadditions could be the trapping of this species by anthracene derivatives such as (1) in Figure 4. Thus, [4+2] cycloaddition of $^1O_2$ to the central anthracene ring would afford an endoperoxide. Depending on the substitution, this endoperoxide (2) could be directly detected or can rearrange with cleavage of the 9− and/or 10−substituent to afford anthraquinone (3), as depicted in Figure 4. The photoreaction could, in principle, be monitored by UV absorption spectroscopy, following the decrease of the characteristic long-wavelength bands of the anthracene chromophore.[87]

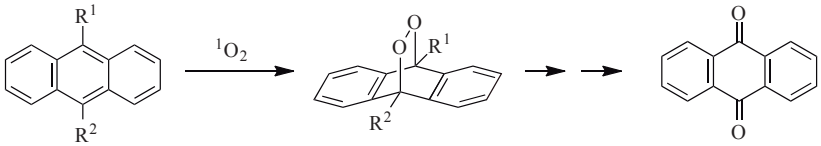

(1) (2) (3)

Figure 4: General reactivity of 9,10-disubstituted anthracenes (1) with formation of an endoperoxide (2) upon addition of singlet oxygen, and rearrangement into an anthraquinone derivative (3).

Conclusions

In summary, we have reported on the near-field magnetic response of different gold nanostructures and investigated their potential application for the enhancement of photochemical processes involving singlet molecular oxygen. In particular, we have focused on the magnetic dipole transitions connecting the triplet $^3\Sigma_g$ and singlet state $^1\Delta_g$ of O_2, which is a good example of dipole-forbidden transition. We have explored the response of single and tip-to-tip welded gold nanorods, which support strong dipolar plasmonic resonances involving large currents flowing along the axis of the nanostructure, and therefore produce strong magnetic fields in their vicinity. These nanoparticles have been designed for providing maximum response when used in liquid suspensions, where customarily photochemical reactions

take place, and for which planar nanostructures are not suitable. Upon rigorous solution of Maxwell's equations we have shown that the studied nanostructures display large magnetic field enhancement factors over significant volumes around them, which enhance both absorption and the emission transitions involving single oxygen. We have also provided a discussion of potential chemical reactions that could be used to detect and monitor the formation of singlet oxygen. The results of this work serve to shed light on the use of plasmonic nanostructures to realize forbidden photochemistry.

Acknowledgement

A.M. acknowledge support from U.S. National Science Foundation (Grant ECCS-1710697). The authors acknowledge the financial support from the following projects: CTQ2014-61671-EXP, MAT2015-69669-P, and PrometeoII/2017/026. We would also like to acknowledge the UNM Center for Advanced Research Computing (CARC) for the computational resources used in this work.

Supporting Information Available

We provide a figure summarizing different chemical reactions of interest for detecting and monitoring singlet oxygen formation.

References

(1) Turro, N.; Ramamurthy, V.; Scaiano, J. *Principles of Molecular Photochemistry: An Introduction*; University Science Books, 2009.

(2) Barron, L. D.; Gray, C. G. The multipole interaction Hamiltonian for time dependent fields. *J. Phys. A* **1973**, *6*, 59.

(3) Craig, D.; Thirunamachandran, T. *Molecular Quantum Electrodynamics: An Introduction to Radiation-molecule Interactions*; Dover Books on Chemistry Series; Dover Publications, 1984.

(4) Maier, S. A. *Plasmonics: Fundamentals and Applications*; Springer: New York, 2007.

(5) Halas, N. J.; Lal, S.; Chang, W.; Link, S.; Nordlander, P. Plasmons in strongly coupled metallic nanostructures. *Chem. Rev.* **2011**, *111*, 3913–3961.

(6) Kneipp, K.; Kneipp, H.; Itzkan, I.; Dasari, R. R.; Feld, M. S. Ultrasensitive Chemical Analysis by Raman Spectroscopy. *Chem. Rev.* **1999**, *99*, 2957–2976.

(7) Zhang, S.; Bao, K.; Halas, N. J.; Xu, H.; Nordlander, P. Substrate-Induced Fano Resonances of a Plasmonic Nanocube: A Route to Increased-Sensitivity Localized Surface Plasmon Resonance Sensors Revealed. *Nano Lett.* **2011**, *11*, 1657–1663.

(8) Zhang, R.; Zhang, Y.; Dong, Z. C.; Jiang, S.; Zhang, C.; Chen, L. G.; Zhang, L.; Liao, Y.; Aizpurua, J.; Luo, Y.; Yang, J. L.; Hou, J. G. Chemical mapping of a single molecule by plasmon-enhanced Raman scattering. *Nature* **2013**, *498*, 82–86.

(9) Bai, W.; Gan, Q.; Bartoli, F.; Zhang, J.; Cai, L.; Huang, Y.; Song, G. Design of plasmonic back structures for efficiency enhancement of thin-film amorphous Si solar cells. *Opt. Lett.* **2009**, *34*, 3725–3727.

(10) Atwater, H. A.; Polman, A. Plasmonics for improved photovoltaic devices. *Nat. Mater.* **2010**, *9*, 205–213.

(11) Mubeen, S.; Lee, J.; Lee, W.-r.; Singh, N.; Stucky, G. D.; Moskovits, M. On the Plasmonic Photovoltaic. *ACS Nano* **2014**, *8*, 6066–6073.

(12) Kamat, P. V. Meeting the Clean Energy Demand: Nanostructure Architectures for Solar Energy Conversion. *J. Phys. Chem. C* **2007**, *111*, 2834–2860.

(13) Linic, S.; Christopher, P.; Ingram, D. B. Plasmonic-Metal Nanostructures for Efficient Conversion of Solar to Chemical Energy. *Nat. Mater.* **2011**, *10*, 911–921.

(14) Hou, W.; Cronin, S. B. A Review of Surface Plasmon Resonance-Enhanced Photocatalysis. *Adv. Funct. Mater.* **2013**, *23*, 1612–1619.

(15) Linden, S.; Enkrich, C.; Wegener, M.; Zhou, J.; Koschny, T.; Soukoulis, C. M. Magnetic Response of Metamaterials at 100 Terahertz. *Science* **2004**, *306*, 1351–1353.

(16) Enkrich, C.; Wegener, M.; Linden, S.; Burger, S.; Zschiedrich, L.; Schmidt, F.; Zhou, J. F.; Koschny, T.; Soukoulis, C. M. Magnetic metamaterials at telecommunication and visible frequencies. *Phys. Rev. Lett.* **2005**, *95*, 203901.

(17) Merlin, R. Metamaterials and the Landau-Lifshitz permeability argument: Large permittivity begets high-frequency magnetism. *Proc. Natl. Academ. Sci.* **2009**, *106*, 1693–1698.

(18) Monticone, F.; Alu, A. The quest for optical magnetism: from split-ring resonators to plasmonic nanoparticles and nanoclusters. *J. Mater. Chem. C* **2014**, *2*, 9059–9072.

(19) Verre, R.; Yang, Z. J.; Shegai, T.; Käll, M. Optical Magnetism and Plasmonic Fano Resonances in Metal-Insulator-Metal Oligomers. *Nano Lett.* **2015**, *15*, 1952–1958.

(20) Shelby, R. A.; Smith, D. R.; Schultz, S. Experimental verification of a negative index of refraction. *Science* **2001**, *292*, 77–79.

(21) Smith, D. R.; Pendry, J. B.; Wiltshire, M. C. K. Metamaterials and negative refractive index. *Science* **2004**, *305*, 788–792.

(22) Soukoulis, C. M.; Kafesaki, M.; Economou, E. N. Negative-Index Materials: New Frontiers in Optics. *Adv. Mater.* **2006**, *18*, 1941–1952.

(23) Zhang, X.; Liu, Z. Superlenses to overcome the diffraction limit. *Nat. Mater.* **2008**, *7*, 435–441.

(24) Schurig, D.; Mock, J. J.; Justice, B. J.; Cummer, S. A.; Pendry, J. B.; Starr, A. F.; Smith, D. R. Metamaterial electromagnetic cloak at microwave frequencies. *Science* **2006**, *314*, 977–980.

(25) Enkrich, C.; Pérez-Willard, F.; Gerthsen, D.; Zhou, J.; Koschny, T.; Soukoulis, C.; Wegener, M.; Linden, S. Focused-Ion-Beam Nanofabrication of Near-Infrared Magnetic Metamaterials. *Adv. Mater.* **2005**, *17*.

(26) Grigorenko, A. N.; Geim, A. K.; Gleeson, H. F.; Zhang, Y.; Firsov, A. A.; Khrushchev, I. Y.; Petrovic, J. Nanofabricated media with negative permeability at visible frequencies. *Nature* **2005**, *438*, 335–338.

(27) Liu, N.; Guo, H.; Fu, L.; Kaiser, S.; Schweizer, H.; Giessen, H. Plasmon Hybridization in Stacked Cut-Wire Metamaterials. *Adv. Mater.* **2007**, *19*, 3628–3632.

(28) Zheludev, N. I. The road ahead for metamaterials. *Science* **2010**, *328*, 582–583.

(29) Liz-Marzán, L. M.; Giersig, M.; Mulvaney, P. Synthesis of Nanosized Gold-Silica Core-Shell Particles. *Langmuir* **1996**, *12*, 4329–4335.

(30) Liz-Marzán, L. M. Tailoring surface plasmon through the morphology and assembly of metal nanoparticles. *Langmuir* **2006**, *22*, 32–41.

(31) Funston, A. M.; Novo, C.; Davis, T. J.; Mulvaney, P. Plasmon Coupling of Gold Nanorods at Short Distances and in Different Geometries. *Nano Lett.* **2009**, *9*, 1651–1658.

(32) Fan, J. A.; Wu, C. H.; Bao, K.; Bao, J. M.; Bardhan, R.; Halas, N. J.; Manoharan, V. N.; Nordlander, P.; Shvets, G.; Capasso, F. Self-Assembled Plasmonic Nanoparticle Clusters. *Science* **2010**, *328*, 1135–1138.

(33) Linden, S.; Enkrich, C.; Dolling, G.; Klein, M. W.; Zhou, J.; Koschny, T.; Soukoulis, C. M.; Burger, S.; Schmidt, F.; Wegener, M. Photonic Metamaterials: Magnetism at Optical Frequencies. *IEEE J. Sel. Topics Quantum Electron.* **2006**, *12*, 1097–1105.

(34) Husnik, M.; Klein, M. W.; Feth, N.; Konig, M.; Niegemann, J.; Busch, K.; Linden, S.; Wegener, M. Absolute extinction cross-section of individual magnetic split-ring resonators. *Nat. Photon* **2008**, *2*, 614–617.

(35) Boudarham, G.; Feth, N.; Myroshnychenko, V.; Linden, S.; García de Abajo, J.; Wegener, M.; Kociak, M. Spectral Imaging of Individual Split-Ring Resonators. *Phys. Rev. Lett.* **2010**, *105*, 255501.

(36) Banzer, P.; Peschel, U.; Quabis, S.; Leuchs, G. On the experimental investigation of the electric and magnetic response of a single nano-structure. *Opt. Express* **2010**, *18*, 10905–10923.

(37) Popa, B.-I.; Cummer, S. A. Compact Dielectric Particles as a Building Block for Low-Loss Magnetic Metamaterials. *Phys. Rev. Lett.* **2008**, *100*, 207401.

(38) Zhao, Q.; Zhou, J.; Zhang, F.; Lippens, D. Mie resonance-based dielectric metamaterials. *Mater. Today* **2009**, *12*, 60 – 69.

(39) Shi, L.; Tuzer, T. U.; Fenollosa, R.; Meseguer, F. A New Dielectric Metamaterial Building Block with a Strong Magnetic Response in the Sub-1.5-Micrometer Region: Silicon Colloid Nanocavities. *Adv. Mater.* **2012**, *24*, 5934–5938.

(40) Kuznetsov, A. I.; Miroshnichenko, A. E.; Fu, Y. H.; Zhang, J.; ; Luk'yanchuk, B. Magnetic light. *Sci. Rep.* **2012**, *2*, 492.

(41) Evlyukhin, A. B.; Novikov, S. M.; Zywietz, U.; Eriksen, R. L.; Reinhardt, C.; Bozhevolnyi, S. I.; Chichkov, B. N. Demonstration of Magnetic Dipole Resonances of Dielectric Nanospheres in the Visible Region. *Nano Lett.* **2012**, *12*, 3749–3755.

(42) Rolly, B.; Bebey, B.; Bidault, S.; Stout, B.; Bonod, N. Promoting magnetic dipolar transition in trivalent lanthanide ions with lossless Mie resonances. *Phys. Rev. B* **2012**, *85*, 245432.

(43) Albella, P.; Poyli, M. A.; Schmidt, M. K.; Maier, S. A.; Moreno, F.; SÃąenz, J. J.; Aizpurua, J. Low-Loss Electric and Magnetic Field-Enhanced Spectroscopy with Subwavelength Silicon Dimers. *J. Phys. Chem. C* **2013**, *117*, 13573–13584.

(44) Baranov, D. G.; Savelev, R. S.; Li, S. V.; Krasnok, A. E.; Alù, A. Modifying magnetic dipole spontaneous emission with nanophotonic structures. *Laser Photon. Rev.* **2017**, *11*, 1600268–n/a.

(45) Feng, T.; Zhou, Y.; Liu, D.; Li, J. Controlling magnetic dipole transition with magnetic plasmonic structures. *Opt. Lett.* **2011**, *36*, 2369–2371.

(46) Hein, S. M.; Giessen, H. Tailoring Magnetic Dipole Emission with Plasmonic Split-Ring Resonators. *Phys. Rev. Lett.* **2013**, *111*, 026803.

(47) Mivelle, M.; Grosjean, T.; Burr, G. W.; Fischer, U. C.; Garcia-Parajo, M. F. Strong Modification of Magnetic Dipole Emission through Diabolo Nanoantennas. *ACS Photonics* **2015**, *2*, 1071–1076.

(48) Ofelt, G. S. Intensities of Crystal Spectra of Rare-Earth Ions. *J. Chem. Phys.* **1962**, *37*, 511–520.

(49) Judd, B. R. Optical Absorption Intensities of Rare-Earth Ions. *Phys. Rev.* **1962**, *127*, 750–761.

(50) Dodson, C. M.; Zia, R. Magnetic dipole and electric quadrupole transitions in the trivalent lanthanide series: Calculated emission rates and oscillator strengths. *Phys. Rev. B* **2012**, *86*, 125102.

(51) Noginova, N.; Barnakov, Y.; Li, H.; Noginov, M. A. Effect of metallic surface on electric dipole and magnetic dipole emission transitions in Eu3+ doped polymeric film. *Opt. Express* **2009**, *17*, 10767–10772.

(52) Karaveli, S.; Zia, R. Spectral tuning by selective enhancement of electric and magnetic dipole emission. *Phys. Rev. Lett.* **2011**, *106*, 193004.

(53) Taminiau, T. H.; Karaveli, S.; van Hulst, N. F.; Zia, R. Quantifying the magnetic nature of light emission. *Nat. Commun.* **2012**, *3*, 979.

(54) Karaveli, S.; Weinstein, A. J.; Zia, R. Direct Modulation of Lanthanide Emission at Sub-Lifetime Scales. *Nano Lett.* **2013**, *13*, 2264–2269.

(55) Noginova, N.; Hussain, R.; Noginov, M. A.; Vella, J.; Urbas, A. Modification of electric and magnetic dipole emission in anisotropic plasmonic systems. *Opt. Express* **2013**, *21*, 23087–23096.

(56) Hussain, R.; Keene, D.; Noginova, N.; Durach, M. Spontaneous emission of electric and magnetic dipoles in the vicinity of thin and thick metal. *Opt. Express* **2014**, *22*, 7744–7755.

(57) Aigouy, L.; Cazé, A.; Gredin, P.; Mortier, M.; Carminati, R. Mapping and Quantifying Electric and Magnetic Dipole Luminescence at the Nanoscale. *Phys. Rev. Lett.* **2014**, *113*, 076101.

(58) Hussain, R.; Kruk, S. S.; Bonner, C. E.; Noginov, M. A.; Staude, I.; Kivshar, Y. S.; Noginova, N.; Neshev, D. N. Enhancing Eu3+ magnetic dipole emission by resonant plasmonic nanostructures. *Opt. Lett.* **2015**, *40*, 1659–1662.

(59) Choi, B.; Iwanaga, M.; Sugimoto, Y.; Sakoda, K.; Miyazaki, H. T. Selective Plasmonic Enhancement of Electric- and Magnetic-Dipole Radiations of Er Ions. *Nano Lett.* **2016**, *16*, 5191–5196.

(60) Álvarez-Puebla, R. A.; Liz-Marzán, L. M.; García de Abajo, F. J. Light concentration at the nanometer scale. *J. Phys. Chem. Lett.* **2010**, *1*, 2428–2434.

(61) Kasperczyk, M.; Person, S.; Ananias, D.; Carlos, L. D.; Novotny, L. Excitation of Magnetic Dipole Transitions at Optical Frequencies. *Phys. Rev. Lett.* **2015**, *114*, 163903.

(62) Filter, R.; Mühlig, S.; Eichelkraut, T.; Rockstuhl, C.; Lederer, F. Controlling the dynamics of quantum mechanical systems sustaining dipole-forbidden transitions via optical nanoantennas. *Phys. Rev. B* **2012**, *86*, 035404.

(63) Kern, A. M.; Martin, O. J. F. Strong enhancement of forbidden atomic transitions using plasmonic nanostructures. *Phys. Rev. A* **2012**, *85*, 022501.

(64) Yannopapas, V.; Paspalakis, E. Giant enhancement of dipole-forbidden transitions via lattices of plasmonic nanoparticles. *J. Mod. Opt.* **2015**, *62*, 1435–1441.

(65) Alabastri, A.; Yang, X.; Manjavacas, A.; Everitt, H. O.; Nordlander, P. Extraordinary Light-Induced Local Angular Momentum near Metallic Nanoparticles. *ACS Nano* **2016**, *10*, 4835–4846.

(66) Rivera, N.; Kaminer, I.; Zhen, B.; Joannopoulos, J. D.; Soljačić, M. Shrinking light to allow forbidden transitions on the atomic scale. *Science* **2016**, *353*, 263–269.

(67) Schweitzer, C.; Schmidt, R. Physical Mechanisms of Generation and Deactivation of Singlet Oxygen. *Chem. Rev.* **2003**, *103*, 1685–1758.

(68) Herzberg, G. Molecular spectra and molecular structure. Vol. 1: Spectra of diatomic molecules. *New York: Van Nostrand Reinhold, 1950, 2nd ed.* **1950**,

(69) Ogilby, P. R. Singlet oxygen: there is indeed something new under the sun. *Chem. Soc. Rev.* **2010**, *39*, 3181–3209.

(70) Ghogare, A. A.; Greer, A. Using Singlet Oxygen to Synthesize Natural Products and Drugs. *Chem. Rev.* **2016**, *116*, 9994–10034.

(71) De Rosa, M. C.; Crutchley, R. J. Photosensitized singlet oxygen and its applications. *Coord. Chem. Rev.* **2002**, *233*, 351 – 371.

(72) Kautsky, H.; de Bruijn, H. Die Aufklärung der Photoluminescenztilgung fluorescierender Systeme durch Sauerstoff: Die Bildung aktiver, diffusionsfähiger Sauerstoffmoleküle durch Sensibilisierung. *Sci. Nat.* **1931**, *19*, 1043–1043.

(73) Foote, C. S.; Wexler, S. Olefin Oxidations with Excited Singlet Molecular Oxygen. *J. Am. Chem. Soc.* **1964**, *86*, 3879–3880.

(74) Grosjean, T.; Mivelle, M.; Baida, F. I.; Burr, G. W.; Fischer, U. C. Diabolo Nanoantenna for Enhancing and Confining the Magnetic Optical Field. *Nano Lett.* **2011**, *11*, 1009–1013.

(75) González-Rubio, G.; González-Izquierdo, J.; Bañares, L.; Tardajos, G.; Rivera, A.; Altantzis, T.; Bals, S.; Peña Rodríguez, O.; Guerrero-Martínez, A.; Liz-Marzán, L. M. Femtosecond Laser-Controlled Tip-to-Tip Assembly and Welding of Gold Nanorods. *Nano Lett.* **2015**, *15*, 8282–8288.

(76) Toftegaard, R.; Arnbjerg, J.; Daasbjerg, K.; Ogilby, P.; Dmitriev, A.; Sutherland, D.; Poulsen, L. Metal-Enhanced 1270?nm Singlet Oxygen Phosphorescence. *Angew. Chem. Int. Ed* **2008**, *47*, 6025–6027.

(77) Wylie, J. M.; Sipe, J. E. Quantum electrodynamics near an interface. *Phys. Rev. A* **1984**, *30*, 1185–1193.

(78) Carminati, R.; Greffet, J.-J.; Henkel, C.; Vigoureux, J. Radiative and non-radiative decay of a single molecule close to a metallic nanoparticle. *Opt. Commun.* **2006**, *261*, 368 – 375.

(79) Novotny, L.; Hecht, B. *Principles of Nano-Optics*; Cambridge University Press: New York, 2006.

(80) García de Abajo, F. J.; Howie, A. Relativistic electron energy loss and electron-induced photon emission in inhomogeneous dielectrics. *Phys. Rev. Lett.* **1998**, *80*, 5180–5183.

(81) García de Abajo, F. J.; Howie, A. Retarded field calculation of electron energy loss in inhomogeneous dielectrics. *Phys. Rev. B* **2002**, *65*, 115418.

(82) Johnson, P. B.; Christy, R. W. Optical constants of the noble metals. *Phys. Rev. B* **1972**, *6*, 4370–4379.

(83) Gao, J.; Bender, C. M.; Murphy, C. J. Dependence of the Gold Nanorod Aspect Ratio on the Nature of the Directing Surfactant in Aqueous Solution. *Langmuir* **2003**, *19*, 9065–9070.

(84) Scarabelli, L.; Sánchez-Iglesias, A.; Pérez-Juste, J.; Liz-Marzáąn, L. M. A 'Tips and Tricks" Practical Guide to the Synthesis of Gold Nanorods. *J. Phys. Chem. Lett.* **2015**, *6*, 4270–4279.

(85) Chigrin, D. N.; Kumar, D.; Cuma, D.; von Plessen, G. Emission Quenching of Magnetic Dipole Transitions near a Metal Nanoparticle. *ACS Photonics* **2016**, *3*, 27–34.

(86) Pohlkötter, A.; Köhring, M.; Willer, U.; Schade, W. Detection of Molecular Oxygen at Low Concentrations Using Quartz Enhanced Photoacoustic Spectroscopy. *Sensors* **2010**, *10*, 8466–8477.

(87) Chadwick, S. J.; Salah, D.; Livesey, P. M.; Brust, M.; Volk, M. Singlet Oxygen Generation by Laser Irradiation of Gold Nanoparticles. *J. Phys. Chem. C* **2016**, *120*, 10647–10657.